nature photonics

REVIEW ARTICLE

PUBLISHED ONLINE: 28 FEBRUARY 2011 | DOI: 10.1038/NPHOTON.2011.309

Chalcogenide photonics

Benjamin J. Eggleton[1]*, Barry Luther-Davies[2] and Kathleen Richardson[3]

The unique and striking material properties of chalcogenide glasses have been studied for decades, providing applications in the electronics industry, imaging and more recently in photonics. This Review summarizes progress in photonic devices that exploit the unique optical properties of chalcogenide glasses for a range of important applications, focusing on recent examples in mid-infrared sensing, integrated optics and ultrahigh-bandwidth signal processing.

Chalcogenide glasses (ChGs) are an important class of amorphous semiconductors used in phase-change memories, solar cells, sensors and photonics. ChGs contain as a major constituent one or more of the chalcogen elements from group 6a of the periodic table (sulphur, selenium and tellurium, but excluding oxygen), covalently bonded to network formers such as As, Ge, Sb, Ga, Si or P. The existence of a broad range of possible glass-forming systems with large composition space and good resistance to crystallization yields glasses with optical properties such as nonlinearity, photosensitivity and infrared transparency, which can all be optimized for photonic applications.

Basic material properties

Research into the optical properties of ChGs started around sixty years ago[1,2]. ChGs are comprised of covalently bonded heavy elements, and this gives them some unique properties for infrared, nonlinear and waveguide optics. Because their inter-atomic bonds are weak relative to those in oxides, the bandgap of ChGs is red-shifted to the visible or near-infrared region of the spectrum. The vibrational energies of the bonds are low because the constituent atoms are particularly heavy. This means that ChGs are transparent into the mid-infrared and, as a consequence, their low phonon energies make them interesting hosts for rare-earth dopants[3,4]. Typically, sulphides transmit to ~11 μm, selenides to ~15 μm and tellurides to beyond 20 μm. However, physical attributes such as the glass transition temperature (T_g), glass hardness, strength and durability generally deteriorate with weaker bonding and therefore decrease with long-wave transparency. A low value of T_g means that precision glass moulding becomes a viable approach for fabricating low-cost optical components for applications such as thermal imaging[2,5]. Glass densities are also high relative to oxide glasses and, when combined with strong polarizability, this leads to a high refractive index of $n \approx 2$–3. A high linear refractive index implies, according to the empirical Miller's rule[6], a high nonlinear refractive index, n_2. This has been confirmed by measurements[7–9] that reveal ultrafast third-order (Kerr) nonlinearities up to a thousand times that of silica, making chalcogenides attractive for all-optical signal processing[10].

The structure of ChGs on the atomic scale is best described as a continuous random network, for which an important parameter is the mean coordination number (MCN) — the sum of the products of the individual abundance times the valency of the constituent atoms. For common binary chalcogenides such as arsenic triselenide (As_2Se_3), the As–Se network is locally two-dimensional with weak van der Waals bonding between the layers. The addition of fourfold-coordinated atoms such as germanium makes the network three-dimensional by creating bonds between layers, increasing network rigidity, T_g, strength and hardness. Covalent bonding leads to a high degree of short-range order, providing well-defined nearest neighbours, bond lengths and bond angles. The relationships between the MCN, network topology and the physical properties of these glasses have been explored by many authors; notably Phillips[11], Thorpe *et al.*[12], Tanaka[13] and Boolchand *et al.*[14]. Thorpe *et al.*[12] showed the existence of a phase transition at MCN = 2.4, providing a percolation threshold between an under-constrained 'floppy' network to an over-constrained 'rigid' phase. Tanaka[13] found that a second phase transition exists at MCN = 2.67, which represents a topological change from a two- to a three-dimensional 'stressed rigid' phase. Boolchand *et al.*[14] suggested the existence of an 'intermediate' phase, representing a self-organized network characterized by zero non-reversing heat flow in measurements using temperature-modulated differential scanning calorimetry. These models are increasingly supported by experimental evidence. An example is the exceptionally large glass-forming range of the Ge–As–Se glass system, in which transitions have been observed in the material density, elastic moduli, index of refraction and bandgap[11–13,15].

If atoms in a continuous random network have fewer or greater numbers of chemical bonds than expected from their valence, then the network will contain coordination defects[16]. The relatively high bond energy and delocalization of the valence and conduction band wavefunctions mean that these defects can exist as pairs with opposite electrical charge — one atom being over-coordinated and the other under-coordinated. These charged defects are 'frozen in' during glass production and are physically separated throughout the glass; if the charges were too close, they would annihilate and change the local chemical bonding. Such defects give rise to 'tail states' in the bandgap that can impact optical and electronic properties, with the number of defects depending on both the form of the material (bulk glass, thin film or fibre) and the preparation method.

One of the most striking properties of ChGs is their photosensitivity — a propensity for the chemical bonds to change when exposed to light with a wavelength near the bandedge[17,18]. Similar changes can also be produced by exposure to heat, X-rays or electron/ion beams. Understanding this phenomenon started with the pioneering work of Ovshinsky[19] and has led to one of the most important applications of chalcogenides: the phase-

[1]Centre for Ultrahigh-bandwidth Devices for Optical Systems, Institute for Photonic Optical Sciences, School of Physics, University of Sydney, New South Wales 2006, Australia. [2]Centre for Ultrahigh-bandwidth Devices for Optical Systems, Laser Physics Centre, The Australian National University, Canberra, Australian Capital Territory 0200, Australia. [3]School of Materials Science and Engineering, COMSET, 161 Sirrine Hall, Clemson University, Clemson, South Carolina 29634, USA. *e-mail: egg@physics.usyd.edu.au

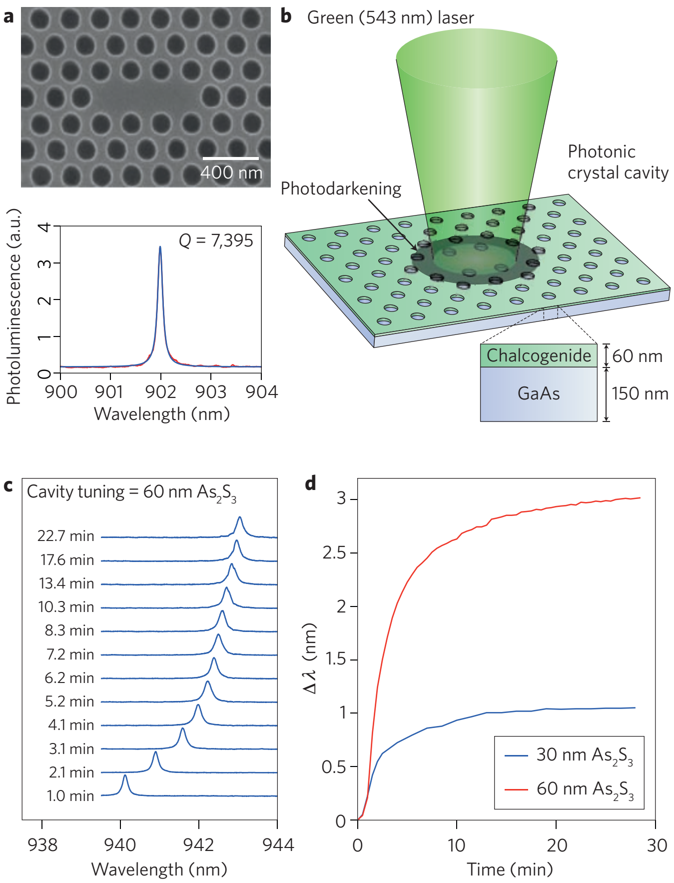

Figure 1 | Use of a photosensitive As_2S_3 chalcogenide film to tune the resonant frequency of a photonic crystal cavity. a, An image of the photonic crystal cavity and its optical response. **b**, Schematic of the method used to tune the cavity. **c**, Cavity response as a function of illumination time for a 60 nm As_2S_3 film. **d**, Tuning curves for two different thicknesses of the As_2S_3 film. Figure reproduced with permission from ref. 32, © 2008 AIP.

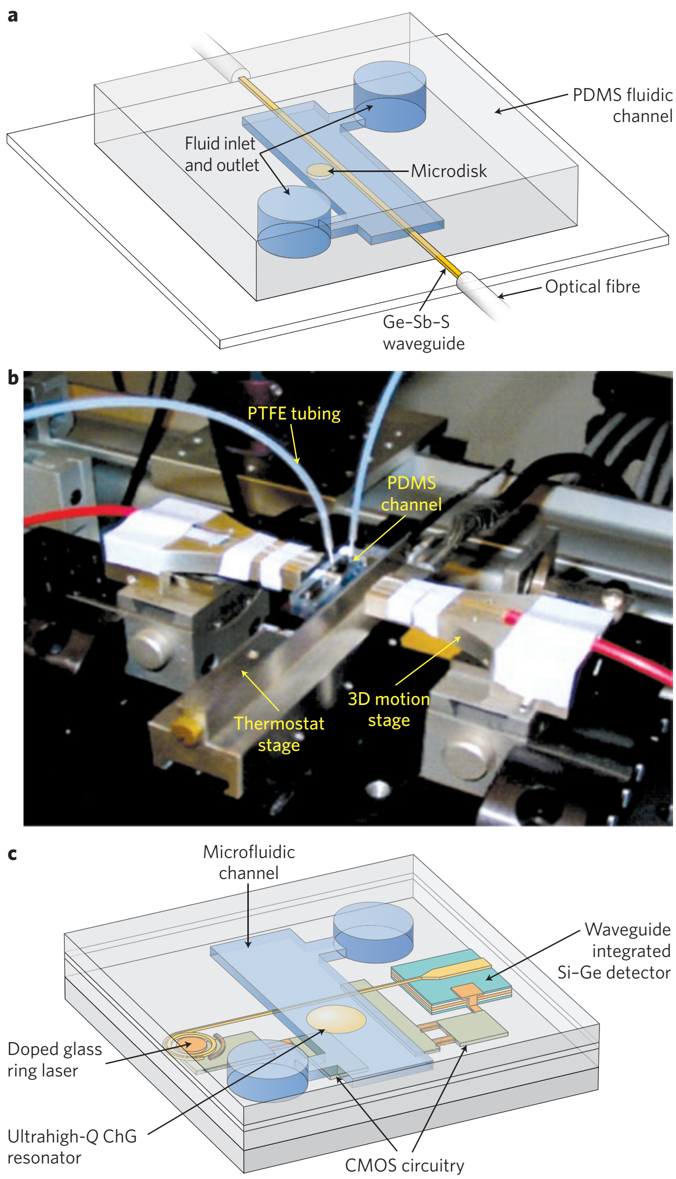

Figure 2 | Structure and testing of a chalcogenide microfluidic sensor. **a**, Schematic of an integrated chalcogenide-based microfluidic sensor. **b**, Experimental realization of the device. **c**, Design of integrated on-chip photonic sensor device. PDMS, polydimethylsiloxane; PTFE, polytetrafluoroethylene; CMOS, complementary metal–oxide–semiconductor. Figure reproduced with permission from ref. 84, © 2010 Wiley.

change memories used in CD/DVD-RW discs and Numonyx memory chips.

The mechanism behind photosensitivity involves the creation of electron–hole pairs, which change the valence of neighbouring atoms and their chemical bonds, thereby creating coordination defects[17]. However, compared with the randomly placed coordination defects described above, these photo-induced states are physically close to each other and can therefore annihilate, restoring either the original bonding or, as a consequence of the steric flexibility of chalcogenides, a different bond configuration. Such bond switching by illumination can result in macroscopic changes in the physical properties of the material, providing a rich range of phenomena that includes photodarkening[20], photodiffusion[21], photofluidity[22] and photocrystallization[23], as well as vectorial effects such as photo-induced birefringence[24]. Many of these effects, although still observable in bulk glasses, become particularly pronounced in thin films. The fabrication of thin films through vapour deposition onto a cold substrate is a non-equilibrium process. Films, therefore, can condense into amorphous states with a large number of defective bonds in molecular clusters, thereby creating a different topology from that of bulk glasses[25]. Photo-excitation creates coordination defects that provide a path through which the amorphous network can relax by bond switching towards a lower energy (bulk-like) state.

Photosensitivity can produce striking changes in the properties of chalcogenide films. For example, although as-deposited thermally evaporated As–S thin films are soluble in amine-based developers, exposure to light near their bandedge or to electrons or high-intensity femtosecond pulses at 800 nm causes the network to polymerize, which strongly affects its solubility. This property has allowed chalcogenide films to be used as electron-beam resists[26] and for the creation of three-dimensional optical nanostructures by femtosecond laser direct writing[27]. Photodarkening is accompanied by a change in refractive index, and this has been used to write waveguides into evaporated films[28], create Bragg gratings in fabricated waveguides[29], tune the wavelength emitted by quantum cascade lasers[30], create high-Q (125,000) cavities in chalcogenide photonic crystals[31], and for post-tuning a photonic crystal cavity made from GaAs to match the emission from embedded quantum dots[32]. This last example is illustrated in Fig. 1, which shows that the photosensitivity of a 30–60-nm-thick As_2S_3 layer could be used

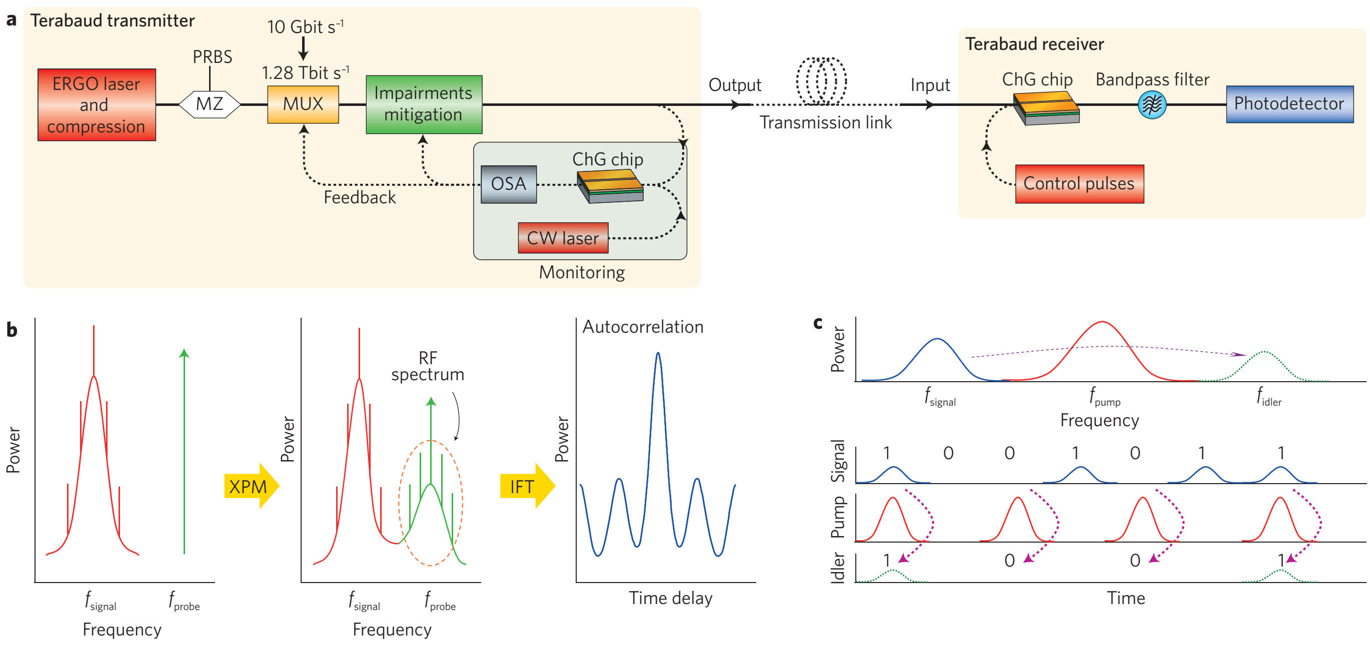

Figure 3 | Use of a chalcogenide photonic chip for transmitter optimization and demultiplexing at 1.28 Tb s^{-1}. a, Diagram of terabaud transmitter optimization and terabaud receiver OTDM demultipexing. **b**,**c**, Schematics of cross-phase-modulation-based RF spectrum analyser for optimizing the optical performance monitor and multiplexer at the transmitter and all-optical terabaud demultiplexing (**c**). ERGO, erbium glass oscillator; MZ, Mach–Zehnder interferometer; PRBS, pseudo-random bit sequence; MUX, multiplexer; OSA, optical spectrum analyser; CW, continuous wave; XPM, cross-phase modulation; IFT, inverse Fourier transform. Figure reproduced with permission from ref. 96, © 2010 OSA.

to tune the resonant frequency of a GaAs photonic crystal cavity by up to 3 nm.

Although photostructural effects in ChGs are a fertile ground for research and applications, they are not necessarily desirable in optical devices exposed to high intensities of light. Photosensitivity has been observed at 1,550 nm in As_2S_3 films[33] — a wavelength well away from the one- or two-photon absorption (TPA) edges. It therefore remains an important question as to whether chalcogenides are stable enough for demanding optical applications such as the delivery of high-power infrared light or all-optical signals processing. In this context, Yang *et al.*[34] recently identified a photostable composition within the family of $Ge_xAs_{45-x}Se_{55}$ glasses at $x \approx 10$, and in glass systems studied for high-power beam delivery compositional tuning has been used to identify glasses with combinations of good infrared transparency, adequate stability and resistance to laser damage. Zhang *et al.*[35] reported laser damage thresholds of 10–20 kW cm^{-2} in low-loss (1–4 dB m^{-1}) multicomponent (Te–As–Se–I and Ga–Sb–Ge–Se) fibres at 9.3 μm that were suitable for CO_2 laser delivery. Similar results have also been reported for CO laser systems[36] and pulsed Er:YAG applications in which damage thresholds of 350 J cm^{-2} at an average power density of 0.5 kW cm^{-2} were realized in low-loss, purified As–S fibres[37]. It is worth noting that in the experiments into all-optical processing summarized below, neither photosensitivity nor optical damage were impediments to achieving high performance.

Chalcogenide fibres and waveguides

The intrinsic transparency window of ChGs, which includes much of the molecular fingerprint region of 2–25 μm, makes them attractive for use in infrared-transmitting optical fibres, and as waveguides for optical sensors and telecommunications.

The first reports of chalcogenide optical fibres in the 1980s[38,39] confirmed that impurity absorption was a major limiting factor for achieving high transparency. Losses remain a general problem for chalcogenides and have limited their use to relatively short fibre lengths (metres). Although the estimated minimum loss in As_2S_3 fibres resulting from Rayleigh scattering is only 4 dB km^{-1} (ref. 40), the lowest value achieved in purified fibres is 23 dB km^{-1} (at 2.3 μm) and more typically lies in the range of 100–200 dB km^{-1} (ref. 41). These elevated values are due to impurity absorption as well as scattering from microscopic bubbles and fragments of silica that become dispersed in the glass during the melting process[42].

Purity is of the utmost importance for maximizing the utility of ChGs, regardless of the final application. Undistilled 'high purity' elemental starting materials often contain finite levels of oxygen, carbon or hydrogen[43,44], with the absorption peaks of these impurities occurring in the range of 1.4–14.9 μm (ref. 45). Reducing impurity levels involves a number of diverse approaches, including heat treatment under vacuum to remove surface oxides[46]; chemical distillation with an oxygen getter[47]; treatment with tellurium halides[48] or reactive chlorine atmospheres[49]; vaporization through porous quartz frits[50]; dynamic pyrolysis[44]; and high-temperature oxidation for purifying sulphur[51]. These allow impurity levels to be reduced to ~10^{-5}% by weight, thus markedly improving infrared transparency.

Several approaches have been used to fabricate optical fibres from ChGs. Step-index fibres can be drawn from 'rod-in-a-tube' preforms produced by core drilling or rotational casting. Core drilling[52,53] can result in increased scattering from interface roughness. Rotational casting can produce preforms with much smoother surfaces than core drilling, but it is a more complex technique, requiring a lathe-mounted mould into which the molten glass is poured and spun during cooling[41,54]. Although other mid-infrared (heavy metal oxide) fibres produced from rotational casting have demonstrated losses as low as 2 dB m^{-1}, such low values have not yet been achieved in ChG fibres. Thus, the 'double crucible technique' is more widely used than rotational casting for production due to the higher resulting glass volatility, which can lead to changes in stoichiometry[55]. Preforms suitable for fabricating step-index fibres have also been produced by extrusion — this leads to low interface roughness and therefore lowers scattering losses[56].

Chalcogenide photonic crystal fibres, which can be either endlessly single mode or provide large/small mode volumes, are an

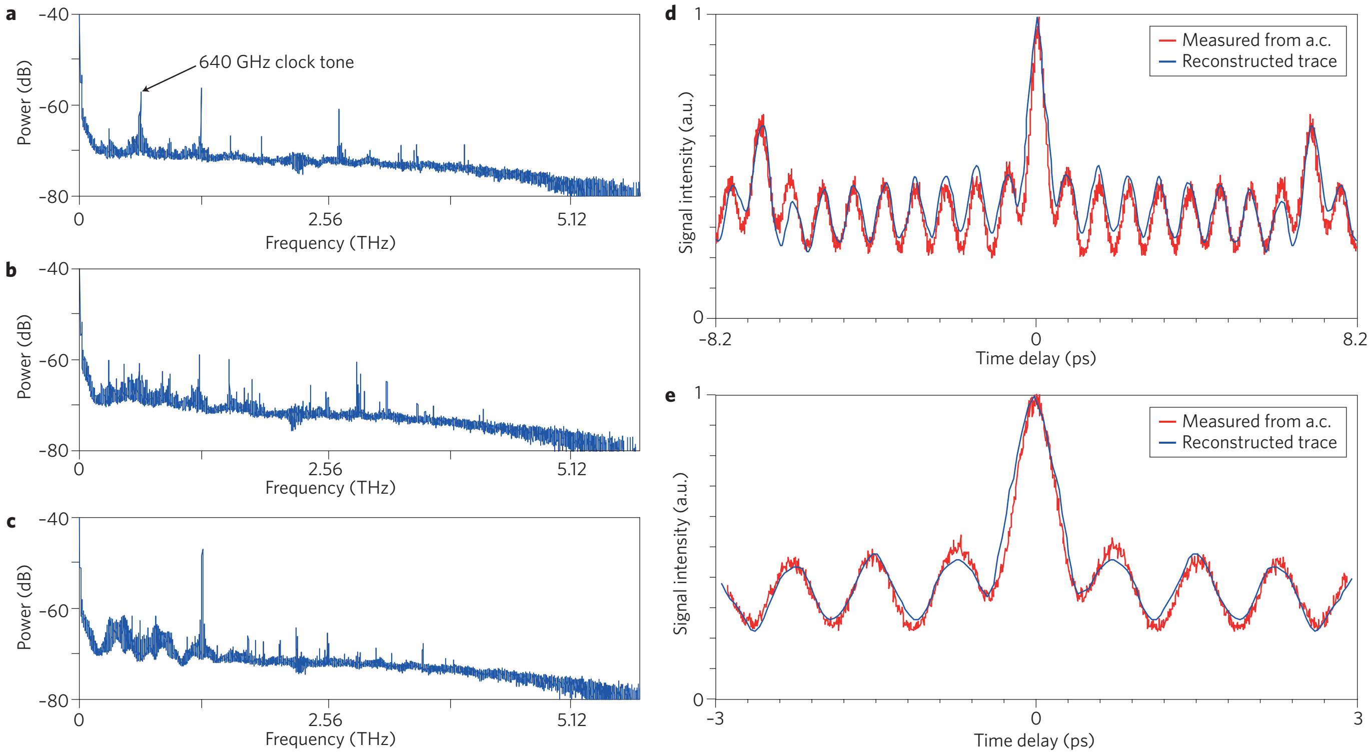

Figure 4 | RF spectra and recovered autocorrelation traces for the unoptimized and optimized transmitter. a–c, Captured RF spectra showing OTDM MUX misalignment (**a**), distortion due to dispersion (**b**) and optimization of the terabaud signal (**c**). **d**,**e**, Reconstructed a.c. waveforms of the unoptimized (**d**) and optimized (**e**) 1.28 Tbit s^{-1} signals. Solid and dotted lines show the a.c. traces measured from the conventional autocorrelator and reconstructed from the captured RF spectra, respectively. Figure reproduced with permission from ref. 96, © 2010 OSA.

attractive alternative to traditional step-index structures because they can be made from a single glass composition. Preforms have been made using both the stack and draw process and through extrusion[57,58]. Hollow-core photonic bandgap omniguide fibres also use chalcogenides and are fabricated from concentric layers of As_2Se_3 and polyethersulfone. They have proven particularly effective for transporting high-power CO_2 laser radiation for applications such as surgery[59]. Other applications of ChG fibres are summarized in ref. 60.

For many applications, optical circuits based on planar waveguides are often preferred over fibres. Chalcogenide glass films for waveguide fabrication have been produced by thermal evaporation[61], sputtering[62], chemical vapour deposition[63] and pulsed laser deposition[64]. For all of these methods, annealing post-deposition is required to relax the chemical bonds towards those of the bulk glass. Several methods for patterning rib or ridge waveguides have been demonstrated. The simplest is to exploit the photosensitivity of chalcogenides by illuminating them near their bandedge, thus photodarkening the material[28,65]. For example, illuminating As_2S_3 films at fluences of around 100 J cm^{-2} at 514 nm or 532 nm typically results in an index change of ~0.04 at 1,550 nm. This index change is sufficient for a single-mode waveguide with a core a few micrometres wide. However, photodefined waveguides can be unstable when heated or exposed to intense light, are difficult to realize in complex multicomponent glasses, and are not easily amenable to dispersion engineering.

A better approach, therefore, is to physically structure the film through lithography and etching to create a rib or ridge waveguide. Early work employed wet chemical etching with NH_4OH to develop the resist patterns and etch the chalcogenide film[28]. However, this is unsatisfactory because the etching is isotropic, leading to poor dimensional control and large sidewall roughness. Anisotropic dry etching or lift-off techniques are therefore preferable. A problem illustrated by the wet etching procedure, however, is that many ChGs are attacked by alkaline resist developers. This has the effect of increasing the roughness of the etched waveguide sidewalls at the nanometre-level, which increases scattering losses.

Lift-off methods, in which the chalcogenide film is deposited onto a pre-patterned resist, circumvent this problem[66]. Surface roughness still remains an issue, however, and methods based on reflow or the application of graded-index coatings have been employed to reduce losses from surface scattering. Losses at 1,550 nm in 800 nm × 400 nm As_2S_3 nanowires were successfully reduced from ~6 dB cm^{-1} to 3.2 dB cm^{-1} by reflow, whereas values as low as 1.5 dB cm^{-1} have been reported for $As_{42}S_{58}$ 1.6 μm × 350 nm waveguides after the application of a graded-index coating — a twofold improvement over uncoated nanowires.

The sensitivity of chalcogenide surfaces to alkaline developers can be overcome by applying a protective coating beneath the resist prior to patterning. Several coatings have been employed so far, with the best results obtained using polymethylmethacrylate (PMMA) or SU-8, which is a chemically amplified epoxy-based negative photoresist. Careful choice of gas chemistry and annealing conditions prior to etching are essential to obtain smooth and vertical sidewalls. For As_2S_3 films the use of CHF_3 gas chemistry for etching results in etched surfaces with a root-mean-squared roughness of ~1.5 nm. The annealing temperature must be limited to ~130 °C to avoid surface degradation and any associated increase in roughness. Standard photolithography and dry etching have been used to produce polymer-clad, dispersion-engineered As_2S_3 rib waveguides measuring 2 μm × 850 nm with losses as low as 0.35 dB cm^{-1} (ref. 67). PMMA is also useful as an electron beam resist when producing chalcogenide nanowires, and was recently used to pattern 530-nm-thick films of highly nonlinear $Ge_{1.5}As_{24.5}Se_{64}$ for producing 630-nm-wide dispersion-engineered waveguides with transverse magnetic losses of ~2.5 dB cm^{-1} (ref. 68).

Table 1 | Nonlinear optical parameters for nonlinear waveguides used for all-optical signal processing.

Device and material	n_2 (m^2 W^{-1})	Nonlinear parameter γ (W^{-1} km^{-1})	Reference	Dispersion coefficient (ps km^{-1} nm^{-1})	Loss (dB m^{-1})	TPA (m W^{-1})	FOM	Free carriers
Highly nonlinear silica fibre	3.2×10^{-20}	21	—	0.03	10^{-3}	Negligible	Large	No
Bismuth oxide fibre	1.1×10^{-18}	1,360	100	−260	0.8	Negligible	Large	No
As_2S_3 fibre	2×10^{-18}	160	101	410	0.88	6.2×10^{-15}	208	No
As_2Se_3 fibre	9×10^{-16}	1,200	102	−504	1	2.5×10^{-12}	2.3	No
As_2S_3 rib waveguide	2.9×10^{-18}	1,700	103	−342	5	6.2×10^{-15}	304	No
As_2Se_3 fibre taper	1.1×10^{-17}	93,400	99	282	<1	2.5×10^{-12}	2.84	No
As_2S_3 dispersion-engineered rib waveguide	3×10^{-18}	9,900	92	29	60	6.2×10^{-15}	312	No
$Ge_{11.5}As_{24}Se_{64.5}$ nanowire	9×10^{-18}	136,000	68	70	250	10^{-13}	60	No
Photonic crystal Ag–As_2Se_3 waveguide	7×10^{-17}	26×10^6	104	Not provided	1,000	$<4.1 \times 10^{-12}$	>11	No
Silicon nanowire waveguide	6×10^{-18}	1.5×10^5	105	Engineered anomalous	400	5×10^{-12}	0.77	Yes

Applications

Sensing. Crystalline chalcogenide materials have been explored as narrow-bandgap semiconductors for photovoltaic infrared imaging. The earliest work from the 1940s was based on PbS, but this quickly expanded to include InSb, PbSe and PbTe (ref. 69). One of the most attractive properties of lead-chalcogenides for infrared imaging — compared, for example, with HgCdTe — is the comparative ease of film deposition, as well as the higher tolerance for compositional inheterogeneities[70]. From a device standpoint, it is preferable to deposit the chalcogenide materials (crystalline detector materials and amorphous components) onto silicon substrates, which are physically robust and can be patterned using standard photolithographic techniques. To accomplish this, a variety of deposition techniques have been employed, including molecular beam epitaxy[71], electrodeposition[72] and ion implantation[73].

ChGs are commonly used in optical sensing platforms, either in fibre or planar form. Fibre-based systems generally operate by exposing a section of the fibre core to the environment to be sensed (liquid or vapour) and monitoring the fibre transmission that is altered by the interaction of the evanescent wave with the medium. This technique is known as fibre evanescent wave spectroscopy[74,75]. Because analyte species are generally organic and so absorb in the mid-infrared, the high transparency of ChGs, along with its availability in fibre form, makes chalcogenide materials attractive for this technique[76]. The hydrophobic surface of the glass itself, along with ease of surface functionalization, leads to high sensitivity[77]. Additionally, it is possible to reduce the diameter of the chalcogenide fibre core, either thermally by heating to a temperature above T_g and then tapering[78], or by chemical etching[79], to increase the system sensitivity.

Recent years have seen significant interest in the use of planar waveguides for chemical sensing. Such waveguides exploit either evanescent wave spectroscopy[80] or Raman spectroscopy[81], and have the advantage of small size, greater reproducibility that fibre devices, and the ability to be monolithically integrated with sources/emitters, detectors and microfluidic analyte delivery systems[61,66]. Waveguide-coupled planar optical resonators have also been demonstrated[82], which provide sensitivities similar to those of commercially available surface-plasmon devices[83], but in a smaller footprint. Figure 2 is a schematic of an enlarged chalcogenide resonator and microfluidic system, showing the entire detection system and the experimental realization[84]. High infrared transparency is the key to achieving high sensitivity. Surface functionalization of the resonator to the analyte(s) produces enhanced selectivity by allowing preferential binding of the species to the surface using, for instance, bacterial antibodies[85]. This flexibility of the sensing platform allows for the detection of multiple species on the same chip.

Devices based on ChGs are also being used in non-optical sensing applications. The detection of heavy metal ions in solution using an 'electronic tongue' is an example of a device that utilizes the solubility of metal ions in a vitreous chalcogenide matrix as its prime functionality, rather than any optical property of the material[86].

Nonlinear effects and all-optical processing. The high material nonlinearity of ChGs, combined with the strong confinement and dispersion engineering achievable in fibre and waveguide devices, makes them attractive as fast nonlinear optical devices. This makes them a good platform for ultrafast nonlinear optics and a key technology for future ultrahigh-bandwidth optical communications systems. For an optical waveguide, the strength of the nonlinear response is characterized by the nonlinear parameter $\gamma = \omega n_2/cA_{eff}$ where A_{eff} is the area of the propagating mode, c is the speed of light and ω is its frequency. The nonlinear phase shift due to the Kerr effect is $\Delta\phi = \gamma PL_{eff}$, where P is the power and L_{eff} is the propagation length, which may be limited by losses, phase matching or pulse walk-off. An important material figure of merit, FOM = $n_2/\beta\lambda$, where β is the TPA coefficient, parameterizes the nonlinear phase shift achievable over one TPA length. Devices used for all-optical processing ideally require FOM > 1. Table 1 compares the parameters of ChG waveguides with those of highly nonlinear silica fibre and silicon nanowires. Chalcogenide devices now offer among the highest values of γ but also benefit from negligible TPA, compared with silicon. This leads to a large FOM and no free-carrier effects, making them an ideal platform for signal processing at ultrahigh bit-rates well beyond the speed of modern electronics. Chalcogenide nanowires can also be dispersion-engineered to provide zero or anomalous dispersion in the telecommunications bands. Such high values of γ allow short device lengths and, when combined with small dispersion, this leads to nonlinear devices with bandwidths of several terahertz[87].

The first demonstrations of nonlinear ChG devices were reported in 1992[88] and used a Kerr shutter or loop mirror based on an As_2S_3 fibre. Strong Kerr nonlinear effects were reported by Lenz *et al.*[89] in Se-based ChGs, and Spalter *et al.*[65] showed strong self-phase modulation in single-mode ChG planar waveguides. Thielen *et al.*[90]

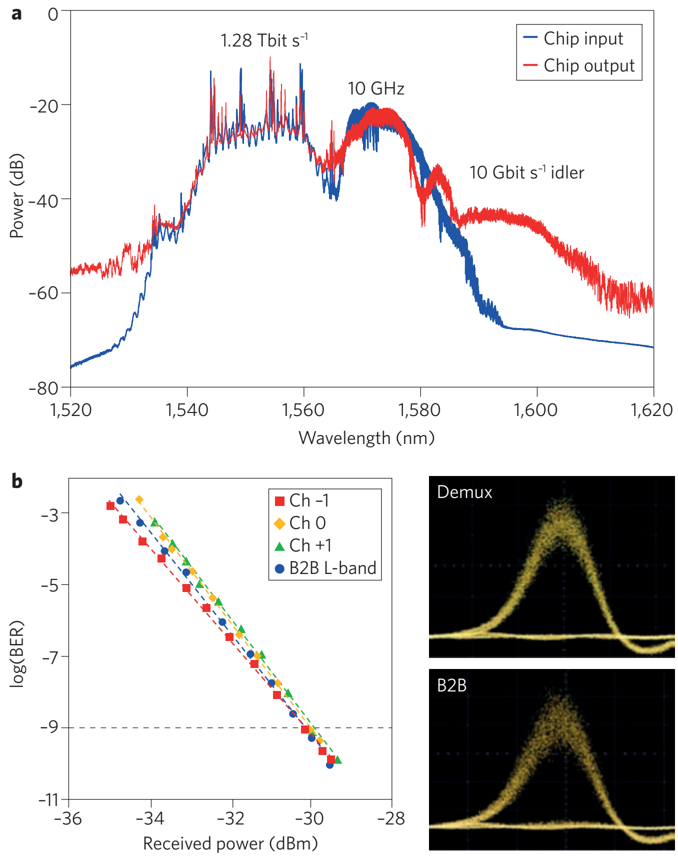

Figure 5 | Performance of the all-optical demultiplexer used to extract individual single data channels at a base rate of 10 Gbit s^{-1} from a 1.28 Tbit s^{-1} signal. a, Optical spectrum at the input and output of the chalcogenide chip. **b**, Bit-error-rate (BER) measurements for three adjacent channels after demultiplexing (demux) compared with back-to-back (B2B) measurements for a 10 Gbit s^{-1} signal in the L-band. Output traces of the B2B and demultiplexed channels are shown on the right. Figure reproduced with permission from ref. 96, © 2010 OSA.

demonstrated 20 dB of Raman gain in a 1.1-m-long As–Se fibre, and Slusher *et al.*[91] measured Kerr nonlinearities nearly 1,000 times higher than those for silica fibres and Raman gains nearly 800 times that of silica. Recently, following the development of nanowires engineered to have anomalous dispersion, ChG waveguides have proven themselves to be efficient broadband generators of supercontinuum light[92,93]. The broad infrared transparency of chalcogenides should also allow the supercontinuum to be extended well into the mid-infrared, and this is now the subject of active research[94].

The large instantaneous Kerr nonlinear response of ChG waveguides allows all-optical processing with large bandwidths. All-optical processors allow single-channel bit-rates in an optical communications system to far exceed the limits imposed by electronics, potentially allowing wavelength-division multiplexing networks to become simpler and more efficient. Over the past five years there have been reports of chalcogenide devices used for regeneration[95], wavelength conversion[10], demultiplexing[96], four-wave-mixing gain[97], optical sampling[98] and performance monitoring[87].

Here we describe an example to illustrate the current state-of-the-art in ChG technology. This involves optical time-division multiplexing (OTDM) to create a single-wavelength data channel at 1.28 terabaud by interleaving 128 channels of 300 fs pulses at a base rate of 10 gigabaud. 1.28 terabaud is equivalent to 1.28 Tbit s^{-1}, which is over 20 times faster than today's commonly available electronic processors. At the end of a link the OTDM signal must be demultiplexed back to the base rate for detection using electronics. A schematic of the system is shown in Fig. 3a. The key signal processing device is a 7-cm-long dispersion-engineered As_2S_3 rib planar waveguide with a nonlinear parameter of $\gamma \approx 9{,}900\ W^{-1}\ km^{-1}$ and a zero-dispersion wavelength close to 1,550 nm. This device has two essential roles: at the transmitter it functions as an optical performance monitor and is used to optimize the multiplexing and compression of the ultrashort pulses; and at the receiver it is used to demultiplex the 1.28 terabaud signal back to the base rate.

The optical performance monitor continuously monitors the quality of the output signal from the transmitter and then generates an error signal that is fed back to optimize the multiplexer and mitigate signal impairments introduced by drift, for example, due to temperature fluctuations. Its working principle is shown in Fig. 3b. When the high-speed OTDM signal co-propagates with a continuous probe, new frequencies are generated around the probe due to cross-phase modulation in the ChG waveguide. These represent the radiofrequency (RF) spectrum of the signal, thus providing detailed information about the signal quality. Impairments may effectively be monitored by exploiting distinguishing features of the RF spectra. The bandwidth of this all-optical RF spectrum analyser is determined by the response time of the underlying nonlinearity (~femtosecond) and the group velocity walk-off between the signal and the probe. These short, dispersion-engineered ChG waveguides provide over a bandwidth of over 3 THz (ref. 87).

Figure 4a–c shows sample RF spectra obtained using this cross-phase-modulation-based RF spectrum analyser. The strong subharmonic peak at 640 GHz in Fig. 4a reveals a misalignment of the multiplexer stages, whereas the low 1.28 THz optical tone in Fig. 4b indicates signal distortion due to dispersion. Figure 4c presents the RF spectrum of a well-optimized 1.28 terabaud output signal.

The working principle of the all-optical demultiplexer is based on four-wave mixing (FWM), as shown in Fig. 3c. The high-bit-rate signal is co-propagated with pump control pulses at the base rate. The pump pulses are adjusted in time to coincide with the desired channel of the high-bit-rate signal, generating a new idler wavelength through FWM that can be extracted from the output by spectral filtering. Figure 5a shows the optical spectra of the 1.28 terabaud source signal and 10 GHz control pulses at the input and output of the waveguide. The high FWM conversion efficiency (~60%) ensures the generation of a high-quality idler signal, as evidenced by the eye diagrams and bit-error-rate measurements shown in Fig. 5b. Although the idler signal seems significantly weaker in the optical spectrum, it should be noted that the duty cycle of the demultiplexed signal is 128 times lower than that of the input signal, corresponding to around a 25 dB reduction in spectral intensity. This highlights the excellent performance achievable with negligible degradation of signal quality and no indication of an error floor in bit-error-rate measurements. It is significant to note that these chalcogenide waveguides operate reliably with continuous power loadings in the 10–20 MW cm^{-2} range.

Conclusions

ChGs offer a unique set of properties among optical glasses that make them an excellent choice for mid-infrared science and nonlinear optics. The research outlined here has not only led to a much better understanding of the material properties that affect the optical performance of chalcogenides, but also illustrates the momentum in the field that has led to the development of high-performance chalcogenide waveguide devices. In this context, chalcogenide nanowires have proven particularly effective for the all-optical processing of high-speed data and low-threshold supercontinuum generation[99]. Following the development of the quantum cascade laser there is renewed interest in waveguide platforms for sensing illicit and dangerous materials through mid-infrared spectroscopy — an area ideally suited to chalcogenide devices. Chalcogenides also provide an excellent platform for integrated interferometers for mid-infrared astronomy, promising to greatly simplifying existing optical systems based on bulk optics. The main challenge for all applications is to identify glasses that have the required stability at high optical fluence — together with adequate transparency and processability — from among the myriad of chalcogenide glass compositions currently available. If achieved, this intriguing range of optical glasses should have an extremely bright future.

References

1. Frerichs, R. New optical glasses with good transparency in the infrared. *J. Opt. Soc. Am.* **43,** 1153–1157 (1953).
2. Hilton, A. R. *Chalcogenide glasses for infra-red optics* (McGraw Hill, 2010).
3. Tver'yanovich, Y. S. & Tverjanovich A. *Rare earth doped chalcogenide glass in semiconducting chalcogenide glass III — Applications of chalcogenide glasses* (eds Fairman, R. & Ushkov, B.) 160–207 (Elsevier, 2004).
4. Sanghera, J. S., Shaw L. B. & Aggarwal, I. D. Chalcogenide glass-fiber-based mid-IR sources and applications. *IEEE J. Sel. Top. Quant.* **15,** 114–119 (2009).
5. Zhang, X. H., Guimond, Y. & Bellec, Y. Production of complex chalcogenide glass optics by molding for thermal Imaging. *J. Non-Cryst. Sol.* **326,** 519–523 (2003).
6. Wang, C. C. Empirical relation between the linear and the third order nonlinear optical susceptibilities. *Phys. Rev. B* **2,** 2045–2048 (1970).
7. Kosa, T. I. *et al.* Nonlinear optical properties of silver-doped As_2S_3. *J. Non-Cryst. Sol.* **166,** 1219–1222 (1993).
8. Harbold, J. M. *et al.* Highly nonlinear As–S–Se glasses for all-optical switching. *Opt. Lett.* **27,** 119–121 (2002).
9. Quemard, C., Smektala, F., Couderc, V., Barthelemy, A. & Lucas, J. Chalcogenide glasses with high nonlinear optical properties for telecommunications. *J. Phys. Chem. Sol.* **62,** 1435–1440 (2001).
10. Pelusi, M. D. *et al.* Applications of highly-nonlinear chalcogenide glass devices tailored for high-speed all-optical signal processing. *IEEE J. Sel. Top. Quant.* **14,** 529–539 (2008).
11. Phillips, J. C. Topology of covalent non-crystalline solids I: Short-range order in Chalcogenide alloys. *J. Non-Cryst. Sol.* **34,** 153–181 (1979).
12. Thorpe, M. F., Jacobs, D. J. & Djordjevic, B. R. The structure and rigidity of network glasses, in insulating and semiconducting glasses (ed. Boolchand, P.) 94–145 (World Scientific, 2000).
13. Tanaka, K. Structural phase transitions in chalcogenide glasses. *Phys. Rev. B* **39,** 1270–1279 (1989).
14. Boolchand, P., Georgiev, D. G. & Goodman, B. Discovery of the intermediate phase in chalcogenide glasses. *J. Opt. Adv. Mat.* **3,** 703–720 (2001).
15. Bulla, D. A. P. *et al.* On the properties and stability of thermally evaporated Ge–As–Se thin films. *App. Phys. A* **96,** 615–625 (2009).
16. Street, R. A. & Mott, N. F. States in the gap in glassy semiconductors. *Phys. Rev. Lett.* **35,** 1293–1296 (1975).
17. Shimakawa, K., Kolobov, A. & Elliott, S. R. Photoinduced effects and metastability in amorphous semiconductors and insulators. *Adv. Phys.* **44,** 475–588 (1995).
18. Fritzsche, H. Light induced structural changes in glasses, in insulating and semiconducting glasses (ed. Boolchand, P.) 653–690 (World Scientific, 2000).
19. Ovshinsky, S. R. Reversible electrical switching phenomena in disordered structures. *Phys. Rev. Lett.* **21,** 1450–1453 (1968).
20. Pfeiffer, G., Paesler, M. A. & Agarwal, S. C. Reversible photodarkening of amorphous arsenic chalcogens. *J. Non-Cryst. Sol.* **130,** 111–143 (1991).
21. Mitkova, M., Kozicki, M. N., Kim, H. C. & Alford, T. L. Thermal and photodiffusion of Ag in S-rich Ge–S amorphous films. *Thin Solid Films* **449,** 248–253 (2004).
22. Calvez , L., Yang, Z. Y. & Lucas, P. Light-induced matrix softening of Ge–As–Se network glasses. *Phys. Rev. Lett.* **101,** 117402 (2008).
23. Kolobov, A. V. & Tominaga, J. Chalcogenide glasses in optical recording: recent progress. *J. Optoelectron. Adv. Mat.* **4,** 679–686 (2002).
24. Krecmer, P. *et al.* Reversible nanocontraction and dilatation in a solid induced by polarized light. *Science* **277,** 1799–1802 (1997).
25. Apling, A., Leadbetter, A. J. & Wright, A. C. Comparison of structures of vapour-deposited and bulk arsenic sulphide glasses. *J. Non-Cryst. Sol.* **23,** 369–384 (1977).
26. Vlcek, M. & Jain, H. Nanostructuring of chalcogenide glasses using electron beam lithography. *J. Optoelectron. Adv. Mat.* **8,** 2108–2111 (2006).
27. Wong, S., Deubel, M., Perez-Willard, F., John, S. & Ozin, G. A. Direct writing of three-dimensional photonic crystals with a complete photonic bandgap in chalcogenide glasses. *Adv. Mat.* **18,** 265–269 (2006).
28. Viens, J.-F. *et al.* Fabrication and characterization of integrated optical waveguides in sulphide chalcogenide glasses. *J. Light. Tech.* **17,** 1184–1191 (1999).
29. Meneghini, C. & Villeneuve, A. As_2S_3 photo-sensitivity by two-photon absorption: holographic gratings and self-written channel waveguides. *J. Opt. Soc. Am. B* **15,** 2946–2950 (1998).
30. Song, S. *et al.* Mode tuning of quantum cascade lasers through optical processing of chalcogenide glass claddings. *Appl. Phys. Lett.* **89,** 041115 (2006).
31. Lee, M. *et al.* Photowritten high-Q cavities in two-dimensional chalcogenide glass photonic crystals. *Opt. Lett.* **34,** 3671–3673 (2009).
32. Faraon, A. *et al.* Local tuning of photonic crystal cavities using chalcogenide glasses. *Appl. Phys. Lett.* **92,** 043123 (2008).
33. Ho, N., Laniel, J. M., Vallée, R. & Villeneuve, A. Photo-sensitivity of As_2S_3 chalcogenide thin films at 1.5 μm. *Opt. Lett.* **28,** 965–967 (2003).
34. Yang, G. *et al.* A photo-stable chalcogenide glass. *Opt. Express* **16,** 10565–10571 (2008).
35. Zhang, X. H., Ma, H. & Lucas, J. Evaluation of glass fibers from the Ga–Ge–Sb–Se system for infrared applications. *Opt. Mater.* **25,** 85–89 (2004).
36. Somkuarnpanit, S. *et al.* Beam delivery characteristics of optical fibers for carbon monoxide lasers. *Opt. Laser Eng.* **23,** 221–231 (1995).
37. Kamensky, V. A., Scripachev, I. V., Snopatin, G. D., Pushkin, A. A. & Churbanov, M. F. High-power As–S glass fiber delivery instrument for pulse YAG:Er laser radiation. *Appl. Opt.* **37,** 5596–5599 (1998).
38. Miyashita, T. & Terunuma, Y. Optical transmission loss of As–S fiber in 1.0–55μm wavelength region. *Jpn. J. Appl. Phys.* **21,** L75–L76 (1982).
39. Hattori, H., Sato, S. & Fujioka, T. High power CO laser transmission through As–S glass fibers. *Electron. Lett.* **20,** 811–812 (1984).
40. Sanghera, J. S. & Aggarwal, I. D. Development of chalcogenide glass fiber optics at NRL. *J. Non-Cryst. Sol.* **213–214,** 63–67 (1997).
41. Sanghera, J. S. *et al.* Development and infrared applications of chalcogenide glass optical fibers. *Fiber Integrated Opt.* **19,** 251–274 (2000).
42. Churbanov, M. F. *et al.* High-purity As-S-Se and As-Se-Te glasses and optical fibers. *Inorg. Mater.* **43,** 441–447 (2007).
43. King, W. A., Clare, A. G. & LaCourse, W. C. Laboratory preparation of highly pure As_2Se_3 glass. *J. Non-Cryst. Sol.* **181,** 231–237 (1995).
44. Susman, S., Rowland, S. C. & Volin, K. J. The purification of elemental sulphur. *J. Mat. Res.* **7,** 1526–1533 (1992).
45. Reitter, A. M., Sreeram, A. N., Varshneya, A. K. & Swiler, D. R. Modified preparation procedure for laboratory melting of multi-component chalcogenide glasses. *J. Non-Cryst. Sol.* **139,** 121–128 (1992).
46. Savage, J. A. Optical properties of chalcogenide glasses. *J. Non-Cryst. Sol.* **47,** 101–116 (1982).
47. Moynihan, C. T., Macedo, P. B., Maklad, M. S., Mohr, R. K. & Howard, R. E. Intrinsic and impurity infrared absorption in As_2Se_3 glass. *J. Non-Cryst. Sol.* **17,** 369–385 (1975).
48. Sanghera, J. S. Process for removing hydrogen and carbon impurities from glasses by adding a tellurium halide. US patent 5,779,757 (1998).
49. Lezal, D., Pedlikova, J., Gurovic, J. & Vogt, R. The preparation of chalcogenide glasses in chlorine reactive atmosphere. *Ceramics* **40,** 55–59 (1996).
50. Hilton, A. R., Hayes, D. J. & Rechtin, M. D. Infrared absorption of some high-purity chalcogenide glasses. *J. Non-Cryst. Sol.* **17,** 319–338 (1975).
51. Adamchik, S. A., Malyshev, A. Y., Bulanov, A. D. & Bab'eva, E. N. Fine purification of sulfur from carbon by high temperature oxidation. *Inorg. Mater.* **37,** 469–472 (2001).
52. Schimmer, R. C. *et al.* Development of germanium gallium sulphide glass fibers for the 1.31 μm praseodymium-doped fiber amplifier. *J. Non-Cryst. Sol.* **284,** 188–192 (2001).
53. McNamara, P. *et al.* Core microstructured fluoride glass optical fiber for mid-infrared single-mode transmission. *J. Non-Cryst. Sol.* **355,** 1461–1467 (2009).
54. Nishii, J. *et al.* Recent advances and trends in chalcogenide glass fiber technology: a review. *J. Non-Cryst. Sol.* **140,** 199–208 (1992).
55. Sanghera, J. S. *et al.* Non-linear properties of chalcogenide glasses and fibers. *J. Non-Cryst. Sol.* **354,** 462–467 (2008).
56. Savage, S. D., Miller, C. A., Furniss, D. & Seddon, A. B. Extrusion of chalcogenide glass preforms and drawing to multimode optical fibers. *J. Non-Cryst. Sol.* **29,** 3418–3427 (2008).
57. Monro, T. M. *et al.* Chalcogenide holey fibers. *Electron. Lett.* **36,** 1998–2000 (2000).
58. Brillad, L. *et al.* Fabrication of complex structures of holey fibers in chalcogenide glass. *Opt. Express* **14,** 1280–1285 (2006).
59. Temelkuran, B. *et al.* Wavelength-scalable hollow optical fibers with large photonic bandgaps for CO_2 laser transmission. *Nature* **420,** 650–653 (2002).
60. Sanghera, J. S., Shaw, L. B. & Aggarwal, I. D. Application of chalcogenide glass optical fibers. *C.R. Chimie* **5,** 873–883 (2002).
61. Hu, J. *et al.* Fabrication and testing of planar chalcogenide waveguide integrated microfluidic sensor. *Opt. Express* **15,** 2307–2314 (2007).
62. Tan, W. C. *et al.* Optical characterization of a-As_2S_3 thin films prepared by magnetron sputtering. *J. Appl. Phys.* **107,** 033524 (2010).

63. Huang, C. C., Hewak, D. W. & Badding, J. V. Deposition and characterization of germanium sulphide glass planar waveguides. *Opt. Express* 2501–2506 (2004).
64. Youden, K. E. *et al.* Pulsed laser deposition of Ga–La–S chalcogenide glass thin film optical waveguides. *Appl. Phys. Lett.* **63,** 1601–1603 (1993).
65. Spalter, S. *et al.* Strong self-phase modulation in planar chalcogenide waveguides. *Opt. Lett.* **27,** 363–365 (2002).
66. Hu, J. J. *et al.* Si-CMOS-compatible lift-off fabrication of low-loss planar chalcogenide waveguides. *Opt. Express* **15,** 11798–11807 (2007).
67. Choi, D.Y. *et al.* Submicrometer thick low loss As_2S_3 planar waveguides for nonlinear optical devices. *IEEE Photon. Tech. Lett.* **22,** 495–497 (2010).
68. Gai, X. *et al.* Dispersion engineered $Ge_{11.5}As_{24}Se_{64.5}$ nanowires with a nonlinear parameter of 136000W^{-1} km^{-1} at 1550nm. *Opt. Express* **18,** 18866–18874 (2010).
69. Rogalski, A. & Piotrowski, J. Intrinsic infrared detectors. *Prog. Quant. Electron.* **12,** 87–289 (1988).
70. Zogg, H. *et al.* Infrared sensor arrays with 3–12 μm cutoff wavelengths in heteroepitaxial narrow-gap semiconductors on silicon substrates. *IEEE Trans. Electron. Dev.* **38,** 1110–1116 (1991).
71. Wu, H. Z. *et al.* Molecular beam epitaxy growth of PbSe on BaF_2-coated Si(111) and observation of the PbSe growth interface. *J. Vac. Sci. Tech.* **17,** 1263–1266 (1999).
72. Xiao, F. *et al.* Electrodeposition of PbTe thin films from acidic nitrate baths. *Electrochim. Acta* **52,** 1101–1107 (2006).
73. Butenko, A. V. *et al.* Characterization of high-temperature PbTe p–n junctions prepared by thermal diffusion and ion implantation. *J. Appl. Phys.* **103,** 024506 (2008).
74. Lucas, P., Riley, M. R., Boussard-Pledel, C. & Bureau, B. Advances in chalcogenide fiber evanescent wave biochemical sensing. *Anal. Biochem.* **351,** 1–10 (2006).
75. Heo, J., Rodrigues, M., Saggese, S. J. & Sigel, G. H. Remote fiber-optic chemical sensing using evanescent-wave interactions in chalcogenide glass fibers. *Appl. Opt.* **30,** 3944–3951 (1991).
76. Anne, M. L. *et al.* Chalcogenide glass optical waveguides for infrared biosensing. *Sensors* **9,** 7398–7411 (2009).
77. Mizaikoff, B. *et al.* Infrared fiber-optical chemical sensors with reactive surface coatings. *Sens. Actuat. B* **29,** 58–63 (1995).
78. Le Coq, D. *et al.* Chalcogenide double index fibers: Fabrication, design, and application as a chemical sensor. *Mat. Res. Bull.* **38,** 1745–1754 (2003).
79. Hocde, S. *et al.* Recent developments in chemical sensing using infrared glass fibers. *J. Non-Cryst. Sol.* **274,** 17–22 (2000).
80. Ganjoo, A. *et al.* Planar chalcogenide waveguides for IR evanescent wave sensor. *J. Non-Cryst. Sol.* **352,** 584–588 (2006).
81. Pope, A. *et al.* Chalcogenide waveguide structures as substrates and guiding layers for evanescent wave Raman spectroscopy of Bacteriorhodospin. *Vib. Spectrosc.* **42,** 249–253 (2006).
82. Hu, J. *et al.* Demonstration of chalcogenide glass racetrack microresonators. *Opt. Lett.* **33,** 761–763 (2008).
83. Hu, J. *et al.* Planar waveguide-coupled, high-index-contrast, high-Q resonators in chalcogenide glass for sensing. *Opt. Lett.* **33,** 2500–2502 (2008).
84. Richardson, K., Krol, D. & Hirao, K. Glasses for photonic applications. *Int. J. Appl. Glass Science* **1,** 74–86 (2010).
85. Ganjoo, A. *et al.* Detection and fingerprinting of pathogens: Mid-IR biosensor using amorphous chalcogenide films. *J. Non-Cryst. Sol.* **354,** 2757–2762 (2008).
86. Vlasov, Y., Legin, A. & Rudnitskaya, A. Cross-sensitivity evaluation of chemical sensors for electronic tongue: determination of heavy metal Ions. *Sens. Actua. B* **44,** 532–537 (1997).
87. Pelusi, M. *et al.* Photonic-chip-based radio-frequency spectrum analyser with terahertz bandwidth. *Nature Photon.* **3,** 139–143 (2009).
88. Asobe, M., Kanamori , T. & Kubodera, K. Ultrafast all-optical switching using highly nonlinear chalcogenide glass fiber. *IEEE Photon. Tech. Lett.* **4,** 362–365 (1992).
89. Lenz, G. *et al.* Large Kerr effect in bulk Se-based chalcogenide glasses. *Opt. Lett.* **25,** 254–256 (2000).
90. Thielen, P. A. *et al.* Small-core As–Se fiber for Raman amplification. *Opt. Lett.* **28,** 1406–1408 (2003).
91. Slusher, R. E., Lenz, G. & Hodelin, J. Laser Raman gain and nonlinear phase shifts in high-purity As_2Se_3 chalcogenide fibers. *J. Opt. Soc. Am. B* **21,** 1146–1155 (2004).
92. Lamont, M. R. E. *et al.* Supercontinuum generation in dispersion engineered highly nonlinear (γ=10/W/m) As_2S_3 chalcogenide planar waveguides. *Opt. Express* **16,** 14938–14944 (2008).
93. El-Amraoui, M. *et al.* Strong infrared spectral broadening in low-loss As–S chalcogenide suspended core microstructured optical fibers. *Opt. Express* **18,** 4547–4556 (2010).
94. Hu, J. *et al.* Maximizing the bandwidth of supercontinuum generation in As_2Se_3 chalcogenide fibers. *Opt. Express* **18,** 6722–6739 (2010).
95. Ta'eed, V. G. *et al.* Self-phase modulation-based integrated optical regeneration in chalcogenide waveguides. *IEEE J. Sel. Top. Quant.* **12,** 360–370 (2006).
96. Vo, T. D. *et al.* Photonic chip based transmitter optimization and receiver demultiplexing of a 1.28 Tbit/s OTDM Signal. *Opt. Express* **18,** 17252–17261 (2010).
97. Lamont, M. R. E. *et al.* Net-gain from a parametric amplifier on a chalcogenide optical chip. *Opt. Express* **16,** 20374–20381 (2008).
98. Van Erps, J. *et al.* High-resolution optical sampling of 640-Gb/s data using four-wave mixing in dispersion-engineered highly nonlinear As_2S_3 planar waveguides. *J. Light. Tech.* **28,** 209–215 (2010).
99. Yeom, D.-I. *et al.* Low-threshold supercontinuum generation in highly nonlinear chalcogenide nanowires. *Opt. Lett.* **33,** 660–662 (2008).
100. Lee, H. *et al.* Bismuth-oxide-based nonlinear fiber with a high SBS threshold and its application to four-wave-mixing wavelength conversion using a pure continuous-wave pump. *J. Light. Tech.* **24,** 22–28 (2006).
101. Asobe, M. *et al.* Third-order nonlinear spectroscopy in As_2S_3 chalcogenide glass fibers. *J. Appl. Phys.* **77,** 5518–5523 (1995).
102. Fu, L. B. *et al.* Investigation of self-phase modulation based optical regeneration in single mode As_2Se_3 chalcogenide glass fiber. *Opt. Express* **13,** 7637–1644 (2005).
103. Madden, S. J. *et al.* Long, low loss etched As_2S_3 chalcogenide waveguides for all-optical signal regeneration. *Opt. Express* **15,** 14414–14421 (2007).
104. Suzuki, K., Hamachi, Y. & Baba, T. Fabrication and characterization of chalcogenide glass photonic crystal waveguides. *Opt. Express* **17,** 22393–22400 (2009).
105. Foster, M. A., Turner, A. C., Lipson, M. & Gaeta, A. L. Nonlinear optics in photonic nanowires. *Opt. Express* **16,** 1300–1320 (2008).

Acknowledgements
The authors thank J.D. Musgraves and T.D. Vo for their help in preparing this manuscript. The support of the Australian Research Council through its Federation Fellowship and Centre of Excellence scheme is also gratefully acknowledged. Funding support related to this effort has been provided to Clemson University by the US Department of Energy under award number DE-SC52-06NA27341 and the National Science Foundation (DMR-0807016).

Additional information
The authors declare no competing financial interests.